PROCEEDINGS OF SCIENCE

Radiation Damage Modelling: TCAD Simulation

Geetika Jain[*†]
Centre for Detector and Related Software Technology,
Department of Physics and Astrophysics, University of Delhi, India.
E-mail: geetika.jain@cern.ch

The exceptional performance of the silicon sensors in the radiation environment has led to their extensive application in high energy physics. Even so, the future experiments foresee these sensors to be exposed to higher radiation levels. Radiation induces a change in the macroscopic properties of the sensor, thus, severely affecting the sensor performance and ultimately becoming the limiting factor for its operation. With an aim to extend the radiation hardness capabilities of the silicon sensors for the future experiments there has been a growing interest in sensors with novel designs and unique characteristic of intrinsic charge multiplication.

However, it is important to understand the effect of radiation damage on these sensors, before employing them in the main detector system. The RD50 collaboration extensively employs TCAD simulation tools for an in-depth understanding and structural optimization of the newly proposed sensor technologies, complementing the measurement results. The simulation package, by the finite element method, solves the Poisson equation coupled with the current continuity equations in the main device, typically with the drift-diffusion current model. There is also the possibility of co-simulating an electronic circuit connected to the main device using the incorporated SPICE package, for example to predict single event effects or read-out related waveforms. The simulation tools also provide an insight into the sensor operation both in the non-irradiated and the irradiated scenario in order to predict the voltage dependence of the leakage current, charge collection and electrical field distribution as function of irradiation. This has required the development of a radiation damage model within the simulation tools such that the measurements are well reproduced. The details of the radiation damage modelling using two commercial TCAD tools Silvaco and Synopsys, are discussed in this work.

The 27th International Workshop on Vertex Detectors - VERTEX2018
22-26 October 2018
MGM Beach Resorts, Muttukadu, Chennai, India

[*]Speaker.
[†]On behalf of the RD50 Collaboration.

© Copyright owned by the author(s) under the terms of the Creative Commons Attribution-NonCommercial-NoDerivatives 4.0 International License (CC BY-NC-ND 4.0).

PoS(VERTEX2018)017

1. Introduction

Silicon detectors are extensively used in high energy physics experiments for particle tracking and vertexing because of their outstanding detection properties and radiation hardness. Since tracking sensors are situated close to the interaction point, they suffer from a high radiation flux of charged particles (protons, pions, etc.) and neutral (neutron and photons) particles. For instance, in order to search for evidence of rare and statistically limited Standard Model and Beyond Standard Model processes, CERN plans an upgrade of the Large Hadron Collider (LHC) to the High Luminosity LHC (HL-LHC) phase [1, 2, 3]. The expected change in the LHC parameters from LHC to HL-LHC phase are listed in Ref. [4]. The conditions in the HL-LHC phase will create an even harsher radiation environment (enormous increase in particle flux) for the different detectors of the experiments, especially for the silicon tracker systems. It is foreseen that the 1 MeV neutron equivalent hadron fluence inside the CMS tracker will be almost ten times more in the HL-LHC phase than the LHC phase [5, 6]. This will lead to an extremely high introduction of crystal defects, causing a corresponding high bulk and surface damage of the silicon sensors, e.g. modification in the electric field distribution, increase of the total leakage current (I_{tot}) and a drastic decrease of the charge collection efficiency (CCE). A long term operation in the radiation environment further degrades the particle detection properties of the silicon sensor [7, 8, 9, 10].

Keeping in mind the challenging radiation environment, its effect on the silicon sensors, the re-

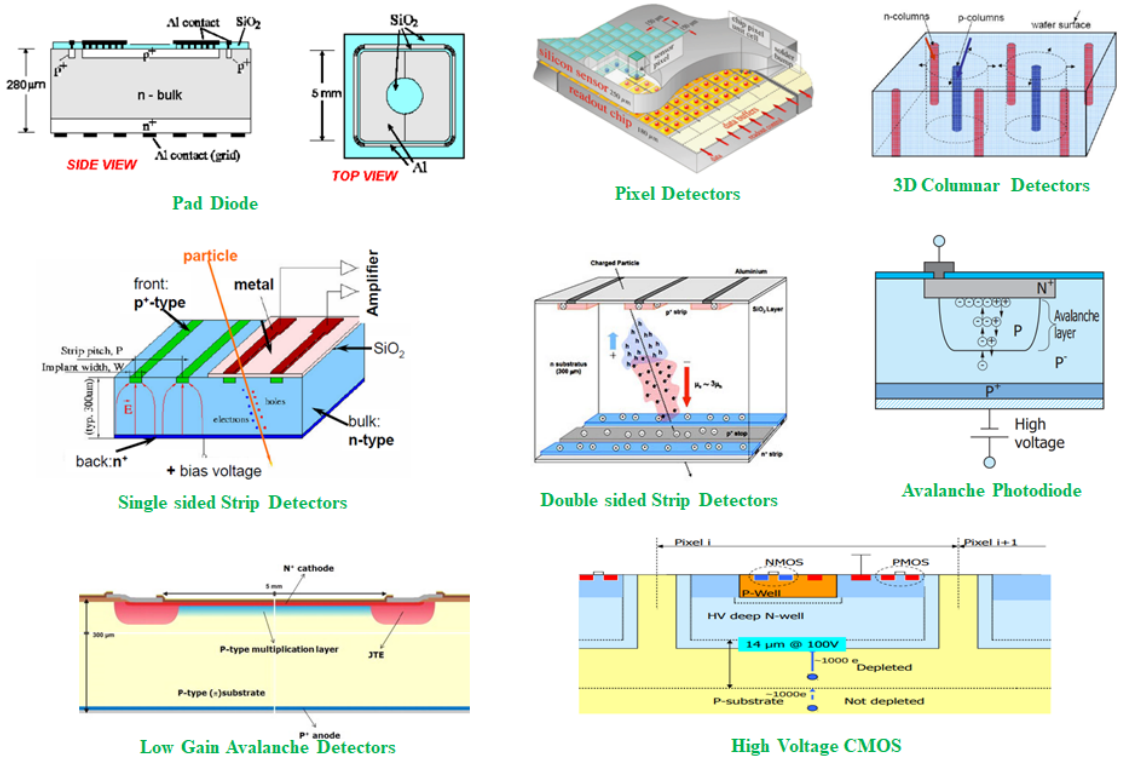

Figure 1: Some of the silicon devices being currently of interest for the high energy physics community.

quirements of future tracker systems; new silicon detector systems that are radiation harder than

PoS(VERTEX2018)017

current detectors have to be designed. A few of the detectors presently used in the experiments and candidates for future experiments are shown in Fig. 1. However, fabrication and evaluating novel designs by implementing real structure designs can be costly and time consuming. Also measurements on real devices may get influenced by unwanted environmental or experimental conditions. Therefore, carrying out simulations can be helpful since they are unaffected by environmental conditions, duration of experiment, and resource availability. Not only this, simulations can provide a better learning handle of the physics inside the detector as the events can be tracked from the initial to the final step. Physics processes (like e.g. impact ionization) can be switched on and off in simulations to better understand how different physical phenomena impact on the detector performance. This leads to an insightful evaluation of the phenomenon taking place at the microscopic level, thereby building a better understanding of the radiation damage mechanism and avoiding design mistakes. Also, simulations allow prediction of the detector operation for change in parameters like bulk material (oxygen enriched Float Zone - FZ, thinned FZ = FTH, deep-diffused FZ - ddFZ, Magnetic Czochralski - MCz or epitaxial material), thickness, polarity (n- or p-type), device design etc. However, it should be noted that simulations cannot replace real devices when it comes to final prototyping and performance tests in complex radiation environments.

2. Simulation framework

A simulation is an imitation of the reality. The physical structure (the dimensions of the structure, the doping profiles, the DC and the AC aluminium contacts, the coupling and the passivation oxide, etc.) has to be mapped into the simulator. A clever choice of the grid points known as the mesh is created on the detector. An appropriate choice of the physical models (for mobility, impact ionization, generation and recombination, oxide physics, Shockley-Read-Hall (SRH) statistics, tunnelling, etc.) is selected, along with the numerical methods (like Newton, Gummel, Block, etc.) to solve the physical equations (Poisson equation, Current density equation and Continuity equation) at the grid points and finally the bias conditions are defined for obtaining the electrical characteristics of the detector. The simulations are tuned to the measured data by different choice of physical models and their parameters, tweaking of process and design parameters. Next, an optimization (in a multi-dimensional parameter phase space) can be carried out as per community requirement. The sensor is then fabricated with the optimized design parameters and tested for macroscopic properties.

There are currently two TCAD device simulators popular in the high energy physics community - Silvaco [11] and Sentaurus [12]. Although the tools used in the Silvaco are described in detail here, the framework is similar for Sentaurus also. Silvaco provides both process and device Technology Computer Aided Design (TCAD) and Electronic Design Automation (EDA) tools. The device TCAD utilizes *DevEdit* as its text editor (in *.in* format) for writing the details of the design and geometry of a semiconductor device. These details are then fed into *Deckbuild*, which is the run time engine and generates a structure file (in *.str* format). *Atlas* is also the TCAD device simulator that enables simulation of electrical and optical behaviour of a semiconductor device. The semiconductor physical models, mobility models, biasing conditions, etc. are implemented through *Atlas* and once again fed to *Deckbuild*. The bulk and surface radiation damage model

PoS(VERTEX2018)017

comprising of set of traps is also implemented, where each trap is defined as a function of energy level (E) depending on trap type (acceptor or donor), trap concentration as a function of fluence (ϕ) and capture cross-sections of electrons and holes (σ_e, σ_h). The surface charges at the silicon-oxide interface are inserted by specifying fixed oxide charge densities (N_{ox}) and interface traps (N_{it}). The MixedMode - an EDA circuit simulator, using electrical circuit models can also be implemented. At this level, two files are generated - (i) a structure file (in *.str* format) containing 2D profiling (3D simulations are also possible) of electric field, potential, electron (hole) concentrations, etc., and (ii) a log file (in *.log* format) consisting information of corresponding current, capacitance, voltage, etc. Silvaco additionally offers Tonyplot - an interactive TCAD tool that provides necessary GUI-based interface for viewing *.str* and *.log* files.

3. Radiation damage modelling

In radiation damage modelling, a minimum number of traps is used instead of using a large number of experimentally found defect complexes (see the spectrum of the Thermally Stimulated Current for defect identification in Fig. 2). The choice of traps is done effectively such that the simulated results describe the change in the electrical behaviour of the detector in the real scenario. In order to avoid a large degree of freedom, the model is usually based on three to five effective traps only. These traps, implemented within the radiation damage model, are tuned such that the simulated results satisfactorily describe the measurement characteristic results like total leakage current (I_{tot}), backplane capacitance (C_{tot}), inter-strip capacitance (C_{int}), inter-resistance (R_{int}), charge collection (CC), etc.

Using the Silvaco software, a combined bulk and surface trap radiation model has been developed

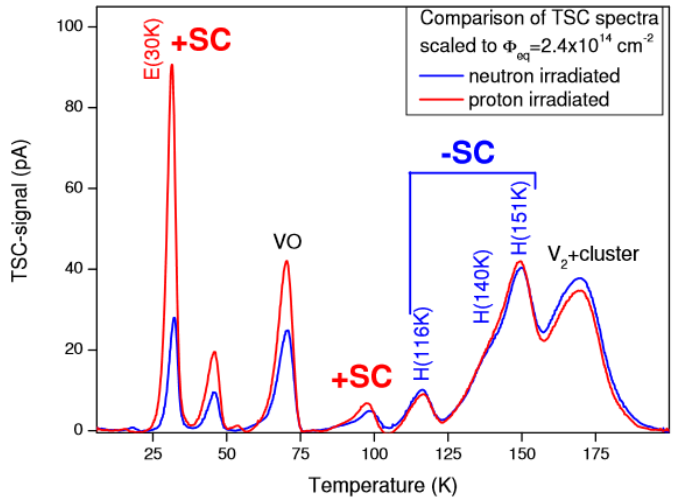

Figure 2: The TSC spectra for n-type oxygen enriched epitaxial silicon diodes show a higher concentration of E(30K) defect for proton irradiation than neutron irradiation. Additionally, the E(30K) defect generates a positive space charge (SC) in the detector bulk. [13].

by Delhi. It consists of - 2 bulk traps, 1 N_{ox}, and 2 N_{it} (see Table 1). Numerous radiation damage models have been built in Sentaurus (see Table 2). All the models are based on the concept of

PoS(VERTEX2018)017

Table 1: Silvaco bulk and surface radiation damage trap model (**Delhi-2014**) for 23 MeV proton irradiation. The detailed modelling and refine tuning of the model and its parameters is described in Ref. [14, 15, 16].

		Fluence ($n_{eq}.cm^{-2}$)	**Density of N_{ox}** (cm^{-3})		
		Non-Irradiated	5×10^{10} to 5×10^{11}		
		1×10^{14}	1×10^{11} to 8×10^{11}		
		5×10^{14}	5×10^{11} to 12×10^{11}		
		1×10^{15}	8×10^{11} to 20×10^{11}		
Damage	**Trap type**	**Energy level** (eV)	**Density** (cm^{-3})	σ_e (cm^2)	σ_h (cm^2)
Bulk	Acceptor	E_C - 0.51	$4 \times \phi$	2.0×10^{-14}	2.6×10^{-14}
Bulk	Donor	E_V + 0.48	$3 \times \phi$	2.0×10^{-14}	2.0×10^{-14}
Interface	Acceptor	E_C - 0.60	$0.6 \times N_{ox}$	0.1×10^{-14}	0.1×10^{-14}
Interface	Acceptor	E_C - 0.39	$0.4 \times N_{ox}$	0.1×10^{-14}	0.1×10^{-14}

Table 2: Various radiation damage trap models in Sentaurus. [17, 18]

Model name	**Trap type**	**Energy level** (eV)	**Density** (cm^{-3})	σ_e (cm^2)	σ_h (cm^2)
Perugia n-type - 2006 [19]	Donor	E_V + 0.36	$1.1 \times \phi$	2.0×10^{-18}	2.5×10^{-15}
	Acceptor	E_C - 0.42	$13 \times \phi$	2×10^{-15}	1.2×10^{-14}
	Acceptor	E_C - 0.50	$0.08 \times \phi$	5×10^{-15}	3.5×10^{-14}
Glasgow - 2008 [20]	Donor	E_V + 0.36	$0.9 \times \phi$	3.23×10^{-13}	3.23×10^{-14}
	Acceptor	E_C - 0.42	$1.613 \times \phi$	9.5×10^{-15}	9.5×10^{-14}
	Acceptor	E_C - 0.46	$0.9 \times \phi$	5×10^{-15}	5×10^{-14}
KIT proton - 2013 [21]	Donor	E_V + 0.48	$5.598 \times \phi$ - 3.949×10^{14}	1.0×10^{-14}	1.0×10^{-14}
	Acceptor	E_C - 0.525	$1.189 \times \phi + 6.454 \times 10^{13}$	1.0×10^{-14}	1.0×10^{-14}
KIT neutron - 2013 [21]	Donor	E_V + 0.48	$1.395 \times \phi$	1.2×10^{-14}	1.2×10^{-14}
	Acceptor	E_C - 0.525	$1.55 \times \phi$	1.2×10^{-14}	1.2×10^{-14}
HIP - 2014 [22]	Donor	E_V + 0.48	$5.598 \times \phi$ - 3.949×10^{14}	1.0×10^{-14}	1.0×10^{-14}
	Acceptor	E_C - 0.525	$1.198 \times \phi + 6.543 \times 10^{13}$	1.0×10^{-14}	1.0×10^{-14}
(2 µm from sur.)	Acceptor	E_C - 0.40	$14.417 \times \phi + 6.543 \times 10^{13}$	8.0×10^{-15}	2.0×10^{-14}
Perugia p-type - 2016 [23]	Donor	E_V + 0.36	$0.9 \times \phi$	3.23×10^{-13}	3.23×10^{-14}
	Acceptor	E_C - 0.42	$1.613 \times \phi$	1.0×10^{-15}	1.0×10^{-14}
($\phi \leq 7.0 \times 10^{15}$)	Acceptor	E_C - 0.46	$0.9 \times \phi$	7.0×10^{-15}	7.0×10^{-14}
($7.0 \times 10^{15} \leq \phi \leq 1.5 \times 10^{16}$)	Acceptor	E_C - 0.46	$0.9 \times \phi$	3.0×10^{-15}	3.0×10^{-14}
($1.5 \times 10^{16} \leq \phi \leq 2.2 \times 10^{16}$)	Acceptor	E_C - 0.46	$0.9 \times \phi$	1.5×10^{-15}	1.5×10^{-14}
Hamburg - 2018 [24]	Donor	E_V + 0.48	$0.5978 \times \phi$	4.166×10^{-15}	1.965×10^{-16}
Hamburg Penta	Donor	E_V + 0.36	$0.3780 \times \phi$	3.230×10^{-17}	2.036×10^{-14}
Trap Model	Acceptor	E_C - 0.545	$0.4335 \times \phi$	4.478×10^{-15}	6.709×10^{-15}
(HPTM)	Acceptor	E_C - 0.458	$0.6447 \times \phi$	2.551×10^{-14}	1.511×10^{-13}
	Donor	E_C - 0.1	$0.0497 \times \phi$	2.300×10^{-14}	2.920×10^{-16}

double-peak electric field in heavily irradiated silicon detectors. Formation of this electric field profile arises from equilibrium carrier trapping on two effective energy levels (E_C - 0.51, acceptor type trap and E_V + 0.48, donor type trap [25]) of radiation-induced defects, which describe changes of detector characteristics under irradiation. It must be noted that there is presently no unique model

PoS(VERTEX2018)017

that can predict behaviour for different sensor materials, particle energy, particle type, effects of annealing, etc.

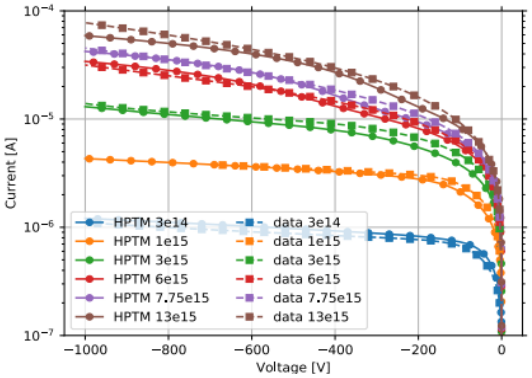

(a)

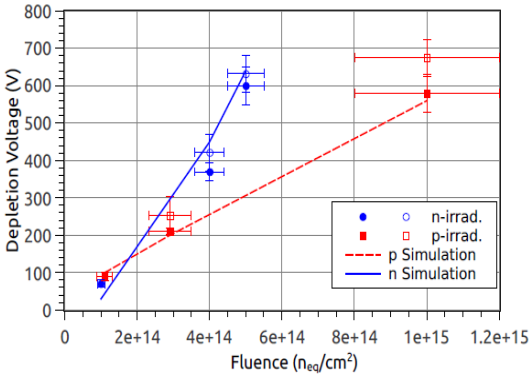

(b)

Figure 3: Comparison of measured and simulated data for - (a) leakage current of FTH200P diodes irradiated with 24 GeV/c protons [24], and (b) full depletion voltage of FZ320N diodes irradiated with 23 MeV protons and reactor neutrons [21].
The simulated radiation damage model used in (a) is *Hamburg-2018* and in (b) is *KIT proton-2013* and *KIT neutron-2013*. (Simulation software used is Sentaurus.)

4. Comparison of simulation results of irradiated sensors with measurements

A mere compilation of experimental observations into simulation commands is not enough, macroscopic results generated from simulations have to be compared to measurement data under similar conditions so as to validate the simulation framework. Based on the observation, various parameters available in the simulation environment, the radiation damage model are further fine tuned.

Fig. 3a shows the simulated and measured leakage current behaviour of FTH200P diodes (thinned p-type float zone diodes of 200 µm thickness) irradiated with 24 GeV/c protons. The diodes were irradiated in the fluence range from 3×10^{14} $n_{eq}.cm^{-2}$ to 1.3×10^{16} $n_{eq}.cm^{-2}$. The

PoS(VERTEX2018)017

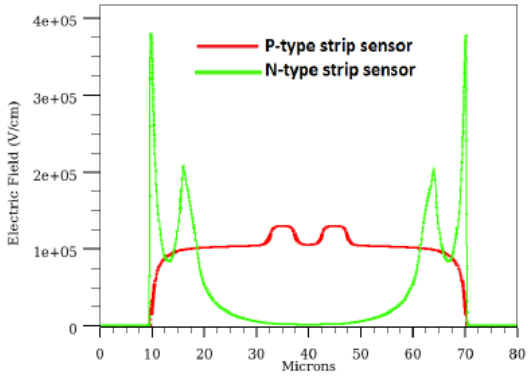

(a)

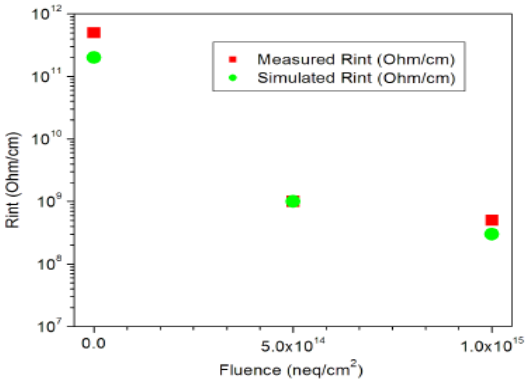

(b)

Figure 4: (a) Simulated electric field at a cutline of 0.1 µm below SiO_2 [26]. (b) Results for R_{int} - measurement and simulation [27]. (Simulation software used is Silvaco, with a combined bulk and surface radiation damage model. The acceptor removal mechanism has not been considered in these simulations.)

leakage current as a function of reverse bias voltage was measured at each fluence. The simulations were performed keeping the same diode parameters and using the *Hamburg Penta Trap Model (HPTM), Hamburg-2018* [24] radiation damage model to simulate radiation damage. It was found that the simulations agree with the measurements within 20% for all fluences and voltages.

The measured and simulated full depletion voltage as a function of fluence for irradiated FZ320N diodes (n-type float zone diodes of 320 µm thickness) is shown in Fig. 3b [21]. The radiation damage simulations use the *KIT proton-2013 and KIT neutron-2013* radiation damage models. The simulated data shows a good match with the measurement results.

The measurements on n- and p-type sensors showed that irradiated n-type sensors exhibit non-gaussian noise earlier than p-type sensors [28]. The reason for this mechanism could not be understood as basic understanding predicts similar behaviour for both n- and p-type sensors. However, insight was provided by the simulated electric field (*Delhi-2014* radiation damage model used), which shows that the electric field increases faster at the implant corners for n- over p-type sub-

PoS(VERTEX2018)017

strates (see Fig. 4a). This occurs because of the acceptor polarity of the surface traps (N_{ox} and N_{it}) which decreases the electric field growth in p-type sensors [27]. This result has been consequential in the change of polarity of sensors from n- to p-type for high fluence experiments [29].

But, all is not well in the operation of p-type sensors. These p-type sensors are prone to loss of inter-strip isolation, i.e. decrease in inter-strip resistance (R_{int}) with increasing fluence. R_{int} is a surface property and so was thought to be affected by surface damage (N_{ox} and N_{it}) only. However, simulation results showed a lower R_{int} as compared to the measurements. It was realised that both surface and bulk damage models (*Delhi-2014*) reproduce correct measured R_{int} values (see Fig. 4b). The explanation for this comes from the fact that the acceptor bulk traps near the n^+ implant are more ionized and therefore compensate the effect of accumulation of electrons by N_{ox} and N_{it} [15].

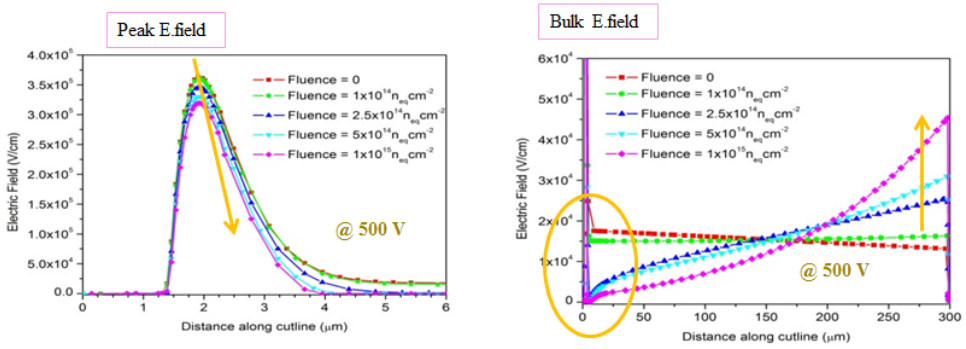

Figure 5: The peak and the bulk electric fields developed in the LGAD detectors at different fluence. The MixedMode of Silvaco and *Delhi-2014* radiation damage model has been used to perform the simulation study.
The LGAD parameters used in this simulation are $\mathbf{N_b} = 1\times10^{12}$ cm^{-3}; $\mathbf{d} = 300\,\mu$m; $\mathbf{N_{im}} = 1\times10^{18}$ cm^{-3}; $\mathbf{d_{im}} = 4\,\mu$m; $\mathbf{N_p} = 9.75\times10^{16}$ cm^{-3}; $\mathbf{d_p} = 7\,\mu$m; $\mathbf{T} = 253$ K; $\mathbf{V} = 500$ V. The details of the study are presented in Ref. [30].

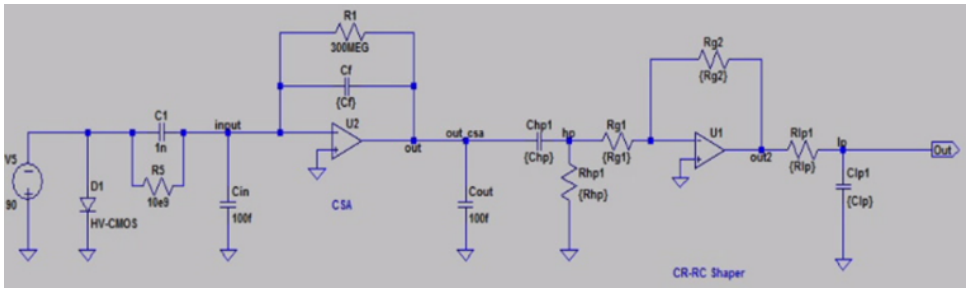

Figure 6: The HV-CMOS device structure built in Sentaurus along with its front-end electronics [31].

5. Digitization of simulations

Simulations with read-out electronics are more realistic and are well suited for Monte Carlo

PoS(VERTEX2018)017

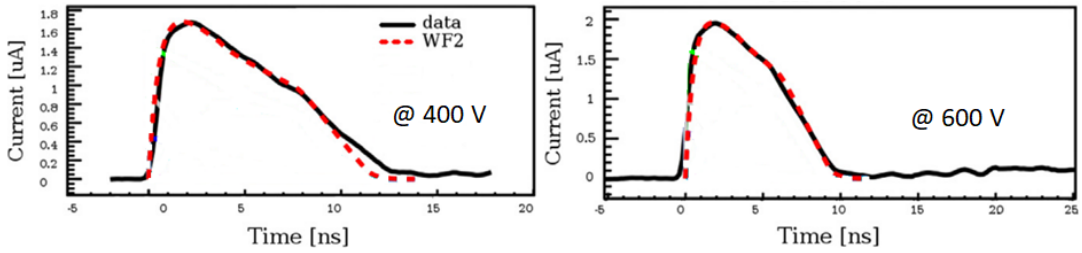

Figure 7: The timing resolution in LGAD devices calculated in Weightfield 2.0 and measured in test beam [32].

studies of detector performance like charge sharing, lorentz angle, position resolution, etc [17]. These device simulations can be further coupled to other software packages e.g. GEANT4 [33], for charge carrier generation distribution. Not only this, these are also suitable for multi-electrode systems since they take weighting fields into account. The possibility of modelling and fitting of the field parameters on the level of source code makes it R&D flexibile. The read-out electronics may either be incorporated at the TCAD device level itself or the TCAD fields have to be imported to other read-out tools. MixedMode in Silvaco [11], MixedMode in Sentaurus [12], Weightfield 2.0 [32], TRACS [34], and Pixelav [35] are a few read-out electronic tools.

The Low Gain Avalanche Detector (LGAD) works on the principle of internal charge multiplication and so has been predicted to be an excellent sensor option for large particle flux experiments. However, it was experimentally observed that the LGAD gain falls drastically with fluence [36, 37]. The electric field profile can not be directly measured, but simulations provide the handle to predict the fields inside the bulk of the sensor. MixedMode simulations have been used to perform the charge collection simulations on the irradiated LGADs. The following set of LGAD parameters has been incorporated in the simulations: uniform bulk doping concentration ($\mathbf{N_b}$) of 1×10^{12} cm^{-3}, detector thickness (**d**) of 300 µm, peak n$^+$ implant concentration ($\mathbf{N_{im}}$) of 1×10^{18} cm^{-3}, n$^+$ implant depth ($\mathbf{d_{im}}$) of 4 µm, peak p-well implant concentration ($\mathbf{N_p}$) of 9.75×10^{16} cm^{-3}, p-well depth $\mathbf{d_p}$ of 7 µm. The charge collection simulation is performed at a temperature **T** of 253 K at a reverse bias voltage **V** of 500 V on different fluence values. The simulated results have provided a plausible explanation to the reduction in the gain. It is observed that the electric field in the multiplication region decreases. Further, with increasing fluence, the high electric field shifts to the backside of the LGAD and drops just below the p-well region to a very low value, leading to an inefficient charge collection (shown in Fig. 5).

Sentaurus offers a similar MixedMode capability, where-in the full front-end electronics is built and then integrated with the device within the TCAD framework. The simulation circuit of the HV-CMOS connected to the bias T, charge sensitive amplifier, and CR-RC shaper is shown in Fig. 6 [31].

Weightfield 2.0 program is based on C++ language and uses ROOT's graphical interface. It employs GEANT4 [33] libraries to simulate the energy loss by the incident particle in silicon. It,

PoS(VERTEX2018)017

then, calculates induced signal currents using the Ramo's theorem. The program provides possibility of input of the following parameters - the sensor design, the p-well gain layer, the type of incoming particle, the presence of an external magnetic field, the operating temperature and reverse bias voltage, etc [32]. The induced current as calculated using Weightfield 2.0 is found to be in excellent agreement with the experimental data as shown in Fig. 7 for 2 bias voltages of 400 and 600 V.

6. Conclusion

TCAD simulation is a powerful tool for investigation of silicon detectors. However, a comparison of the measurements with TCAD simulations is important to tune the models and the various simulation parameters. The simulation of the radiation damage is a challenge that satisfactorily describes the whole set of measurements is not yet available. Also there is a need to develop a model suitable for different set of detectors and irradiations which will be helpful in understanding the behaviour of the novel detectors and design optimization.

7. Acknowledgement

Authors are thankful to the RD50 Collaboration, the VERTEX 2018 workshop, the University of Delhi R&D grant, the DST for research and financial support.

References

[1] CMS Collaboration. *Technical Proposal for the Phase-II Upgrade of the CMS Detector*, CERN-LHCC-2015-010, LHCC-P-008, CMS-TDR-15-02 (2015).

[2] CMS Collaboration. *Updates on Performance of Physics Objects with the Upgraded CMS detector for High Luminosity LHC*, CMS-DP-2016-065 (2016).

[3] CMS Collaboration. *Updates on Projections of Physics Reach with the Upgraded CMS Detector for High Luminosity LHC*, CMS-DP-2016-064 (2016).

[4] Andreas Hoecker. *Physics at the LHC Run-2 and Beyond*, CERN Yellow Reports: School Proceedings Archives 5 (2017).

[5] S. Mallows. BRIL webpage https://twiki.cern.ch/twiki/bin/viewauth/CMSPublic/BRILRSelbaHGC.

[6] M. Guthoff. BRIL webpage https://twiki.cern.ch/twiki/bin/view/CMSPublic/BRILRS1D1MeVneqAtTracker.

[7] G. Casse et al. *New operation scenarios for severely irradiated silicon detectors*, PoS(Vertex)008 (2009).

[8] M. Moll. *Development of Radiation Tolerant Silicon Sensors - A Status Report of the RD50 Collaboration*, PoS(Vertex)026 (2013).

[9] G. Kramberger et al. *Comparison of pad detectors produced on different silicon materials after irradiation with n, p & pions*, *NIM A* **612** (2010) 288 - 295.

[10] A. Affolder et al. *Collected charge of planar silicon detectors after pion and proton irradiations up to* $2.2 \times 10^{16}\ n_{eq}.cm^{-2}$, *NIM A* **623** (2010) 177 - 179.

PoS(VERTEX2018)017

[11] ATLAS Silvaco version 5.15.32.R Nov 2009. *Users manual*, Silvaco webpage. http://www.silvaco.com

[12] Sentaurus TCAD Industry–Standard Process and Device Simulators, Synopsys documentation. http://www.synopsys.com.

[13] A. Junkes. *Status of defect investigations*, PoS(Vertex)035 (2011).

[14] CMS Detector Note. *Simulation of Silicon Devices for the CMS Phase II Tracker Upgrade*, CMS DN-2014/016.

[15] R. Dalal, G. Jain, A. Bhardwaj, K. Ranjan. *Simulation of Irradiated Si Detectors*, POS(Vertex)030 (2014).

[16] R. Dalal. *Performance Characteristics of Si Sensors at Collider Experiments*, Ph.D. Thesis, University of Delhi (2015).

[17] G. Kramberger. *Radiation damage models, comparison and performance of TCAD simulation*, POS(Vertex)034 (2016).

[18] M. Moll. *Displacement Damage in Silicon Detectors for High Energy Physics*, IEEE **65** (2018) 8.

[19] M. Petasecca, et al. *Numerical simulation of radiation damage effects in p-type and n-type FZ silicon detectors*, IEEE **53** (2006) 5, 2971-2976.

[20] D. Pennicard et al. *Simulations of radiation-damaged 3D detectors for the Super-LHC*, NIM A **592** (2008) 16-25.

[21] R. Eber. *Investigations of new sensor designs and development of an effective radiation damage model for the simulation of highly irradiated silicon particle detectors*, Ph.D. Thesis, Karlsruhe Institute of Technology (2001).

[22] T. Peltola. *Simulation of radiation-induced defects*, PoS(Vertex)031 (2015).

[23] F. Moscatelli et al. *Combined bulk and surface radiation damage effects at very high fluences in silicon detectors: Measurements and TCAD simulations*, IEEE **63** (2016) 5, 2716-2723.

[24] J. Schwandt. *A new model for the TCAD simulation of the silicon damage by high fluence proton irradiation - The Hamburg Penta Trap Model*, 32^{nd} RD50 Workshop (2018).

[25] V. Eremin, E. Verbitskaya, Z. Li. *The origin of double peak electric field distribution in heavily irradiated silicon detectors*, *NIM A* **476** (2002) 556-564.

[26] R. Dalal. *Comparison of Radiation Hardness Properties of p+n- and n+p- Si Strip Sensors Using Simulation Approach*, 23^{rd} RD50 Workshop (2013).

[27] R. Dalal. *Simulations for Hadron Irradiated n+p- Si Strip Sensors Incorporating Bulk and Surface Damage*, 23^{rd} RD50 Workshop (2013).

[28] A. Dierlamm. *Silicon sensor developments for the CMS Tracker upgrade*, JINST 7 (2012).

[29] CMS Collaboration. *The Phase-2 Upgrade of the CMS Tracker Technical Design Report*, CERN-LHCC-2017-009, CMS-TDR-17-001 (2017).

[30] R. Dalal, G. Jain, A. Bhardwaj, K. Ranjan. *TCAD simulation of Low Gain Avalanche Detectors*, NIM A **836** (2016) 113 - 121.

[31] F. R. Palomo. *TCAD Simulations HV-CMOS AMS 0.35 um Reach-Through Diode*, 27^{th} RD50 Workshop (2015).

PoS(VERTEX2018)017

[32] F. Cenna et al. *A fast simulator for silicon and diamond solid state detector*, NIM A **796** (2015) 149-153.

[33] S. Agostinelli, et al. *Geant4 - A simulation toolkit*, NIM A **506** (2003) 250.

[34] J. Calvo, et al. *TRACS: A multi-thread transient current simulator for micro strips and pad detectors*, NIM A **917** (2019) 77-85.

[35] M. Swartz. *CMS pixel simulations*, NIM A **511** (2003) 88-91.

[36] G. Kramberger. *Radiation hardness of Low Gain Amplification Detectors (LGAD)*, 24^{th} RD50 Workshop (2014).

[37] G. Dalla Betta et al. *Design and TCAD simulation of double-sided pixelated low gain avalanche detectors*, NIM A **796** (2015) 154 - 157.

PoS(VERTEX2018)017